

Signal and noise in magneto-optical readout

Cite as: Journal of Applied Physics **53**, 4485 (1982); <https://doi.org/10.1063/1.331185>
Published Online: 04 June 1998

Masud Mansuripur, G. A. N. Connell, and Joseph W. Goodman



[View Online](#)



[Export Citation](#)

ARTICLES YOU MAY BE INTERESTED IN

[Magneto-Optical Effects](#)

Journal of Applied Physics **38**, 1482 (1967); <https://doi.org/10.1063/1.1709678>

[Magneto-Optic Scattering from Thin Solid Films](#)

Journal of Applied Physics **38**, 1652 (1967); <https://doi.org/10.1063/1.1709738>

[Magnetic susceptibility measurements of ultrathin films using the surface magneto-optic Kerr effect: Optimization of the signal-to-noise ratio](#)

Review of Scientific Instruments **68**, 4212 (1997); <https://doi.org/10.1063/1.1148368>

Ultra High Performance SDD Detectors



See all our XRF Solutions

Signal and noise in magneto-optical readout

Masud Mansuripur and G. A. N. Connell

Xerox Corporation, Palo Alto Research Center, 3333 Coyote Hill Road, Palo Alto, California 94304

Joseph W. Goodman

Department of Electrical Engineering, Stanford University, Stanford, California 94305

(Received 16 November 1981; accepted for publication 26 January 1982)

For a magneto-optical readout system which uses the Kerr effect, the power spectral density of the read signal has been derived. The noise components originating in the photodetection and amplification stages appear as additive terms in the expression for the overall spectral density, enabling us to define a signal to noise ratio for the readout system. Adjustable parameters of the system are then optimized and a multilayer disk structure is introduced which enhances the Kerr effect and, consequently, results in an increased signal to noise ratio.

PACS numbers: 85.70.Sq

I. INTRODUCTION

Presently up to a million bits of information can be stored per square inch on conventional magnetic disk media. The upper limit on the storage density is set by the sensitivity of the read-write head rather than by the magnetic properties of the media, particularly when vertical as opposed to in-plane recording is considered. Thus, new methods providing access to smaller regions of magnetic film, could provide marked improvements in storage density. In principle, the ability to focus laser light to sufficiently small dimensions offers an attractive solution to this problem, as well as a way of exploiting the optical and thermal properties of perpendicular media to store, erase, and retrieve information at densities approaching the media limits. The possibilities and realization of this approach are therefore of considerable interest.^{1,2}

In this paper, we will discuss the read signal from a magneto-optical disk when the polar Kerr effect is used, reserving the problem of the writing and erasure of data for a later publication. The polar Kerr effect itself is observed by the changes in the state of polarization of light that occur after normal reflection from a perpendicularly magnetized medium. Figure 1, therefore, represents the simplest system that can use this effect to extract data from a magneto-optical disk. The magnetic film has perpendicular anisotropy, and the direction of magnetization (either up or down) in any region determines whether a zero or one is encoded there. When linearly polarized light is normally incident on the film, the rotation of the major axis from the original polarization direction and the ellipticity of the polarized reflected light both have signs that depend on the direction of magnetization. Thus, the polarization analyzer shown converts major axis rotations to changes in light intensity which are then converted to electric current variations by a photodetector. The addition of a quarter wave plate at Q would permit changes of ellipticity to be detected in the same way.

The polar Kerr effect is usually very small. Typically the rotation angle and the ellipticity of the reflected light are of the order of 0.1 degrees. Thus, with the simple detector of Fig. 1, the information-carrying signal would be but a small fraction of the detected signal. To improve on this situation,

two approaches have been taken. The first is to use the differential detection scheme of Fig. 2.³ In this scheme, the reflected light is split in two halves and each half is detected by a separate detector. The detectors are identical except for the setting of the analyzers. The null axis of one analyzer is set at angle $+\theta$ with respect to the unrotated polarization vector, while the other is set at $-\theta$. When the two outputs are fed to a differential amplifier, the dc components cancel each other and the amplified signal is received at the output. This signal is processed by a filter before reaching the decision point. The second approach is to enhance the rotation angle or the ellipticity through interference effects that occur when, for example, the sample is overcoated with a thin dielectric film. Our aim is to find the conditions that make best use of these elements when used together. Thus, in this paper we first focus on the performance of the differential detection scheme itself. Then, we consider how interference effects enhance the magneto-optic response and so find that

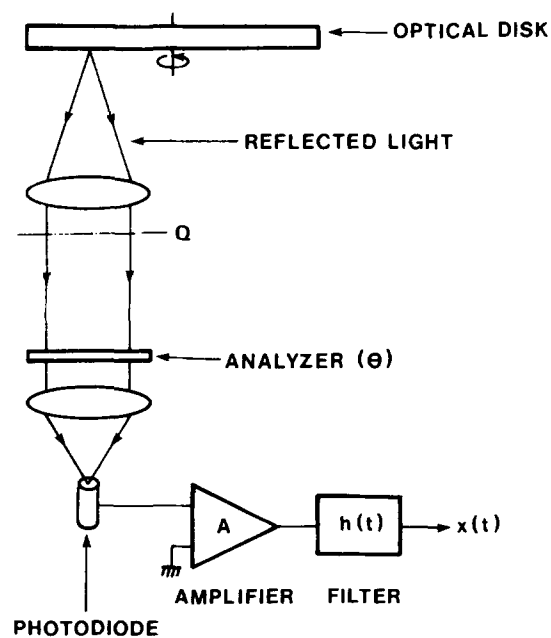


FIG. 1. Schematic diagram of a simple readout system.

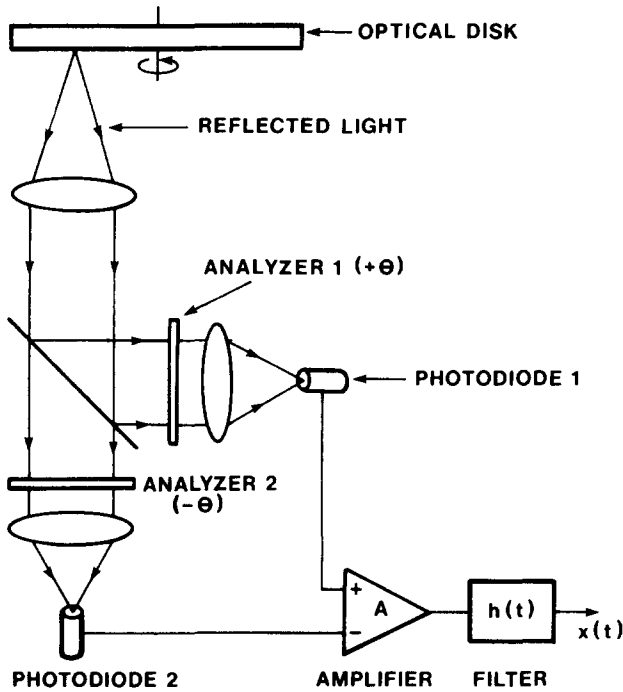


FIG. 2. Schematic diagram of a differential readout system.

multilayer device that results in maximum signal to noise ratio when used with the differential detection scheme.

The paper is organized as follows. Section II is a brief account of the polar Kerr effect that provides both an intuitive view of how interference schemes can improve the response of the magneto-optic medium and the mathematical framework for magneto-optic calculations on multilayer devices. This is a basis for the derivation of the power spectral density of the read signal from the differential detection system in Sec. III and of the signal to noise ratio in Sec. IV. The signal to noise ratio in a digital detection system is directly related to error rates only when the noise is additive and Gaussian, which is not exactly the case in this problem. An exact evaluation of the system should therefore be based on a more complicated analysis. We have shown elsewhere,⁴ however, that in a conventional photodetection system the assumption of Gaussian statistics yields reasonably accurate predictions. Therefore the signal to noise ratio is a good measure of achievable error rates. Results of Sec. IV are then used in Sec. V to obtain the optimum disc structure and maximum signal to noise ratio for the differential detection system. Our conclusions are summarized in Sec. VI.

II. THE POLAR KERR EFFECT

The polar Kerr effect occurs when light is reflected normally from a perpendicularly magnetized medium. Under these conditions, it is readily shown⁵ that the normal modes of propagation are right (a^-) and left (a^+) circularly polarized with eigenvalues:

$$n^\pm = (\epsilon \pm i\epsilon')^{1/2}. \quad (1)$$

In this equation, ϵ and ϵ' are the complex diagonal and off-diagonal elements of the dielectric tensor, which are even and odd functions of magnetization, respectively. For iso-

tropic, non-magnetic materials, it therefore follows that $\epsilon' = 0$ and $n^+ = n^- = \epsilon^{1/2}$, i.e., the usual relationship between refractive index and dielectric constant.

It is often convenient experimentally to use linearly polarized light for the observation of the Kerr effect. In this case, with the incident light linearly polarized along the X direction, the reflected light has the regular component r_x and a magneto-optically induced component r_y , where r_x and r_y are complex. The magnitude of the polar Kerr effect, $|r_y|$, is determined both by the internal convertivity⁶ of the medium set by ϵ' , and by the ability to introduce light into and remove magneto-optic radiation from the medium such that maximum conversion, as measured outside the medium, occurs. This latter aspect is very much affected by interference effects within the device structure and considerable enhancement of $|r_y|$ over its value for a bulk sample can be obtained. For example, the simplest case of a dielectric anti-reflection coating on a bulk material produces a small gain because more light enters the magnetic medium. It is not effective, however, either in increasing the efficiency of conversion within the magnetic medium itself or in increasing the collection of the magneto-optic radiation. Consider, however, the device shown in Fig. 3 in which the magnetic thin film is deposited on a transparent dielectric film that itself rests on an opaque reflector, to form what may be called a trilayer device. The thicknesses of the sample and transparent dielectric films are adjusted so that $r_x = 0$. This occurs because the ray reflected directly by the sample is exactly cancelled by light which has suffered at least one reflection from the back reflector. To achieve this, the optical thickness of the dielectric layer must be approximately $(2m + 1)\lambda/4$, where λ is the wavelength of the light used in the magneto-optic experiment and $m = 0, 1, \text{etc.}$ (In actual practice, $m = 0$ is adequate for most purposes.) Therefore, when a perfect opaque reflector is used, all of the incident intensity is absorbed in the thin absorbing sample. Furthermore, magneto-optically induced light (ELX), which is emitted both forwards and backwards from the sample, suffers relatively little reabsorption in the thin absorbing film, and the interference conditions that have been set up to create total absorption of the incident beam are exactly those required to maximize $|r_y|$ by in-phase addition of the exiting

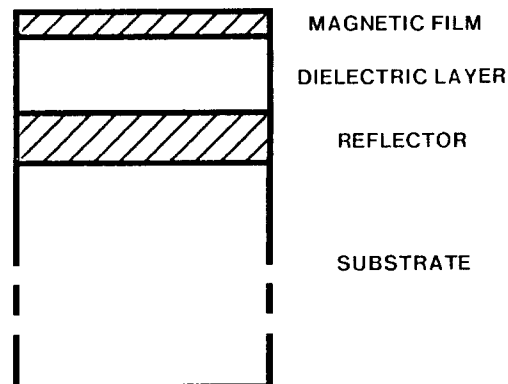


FIG. 3. Trilayer structure for magneto-optic device.

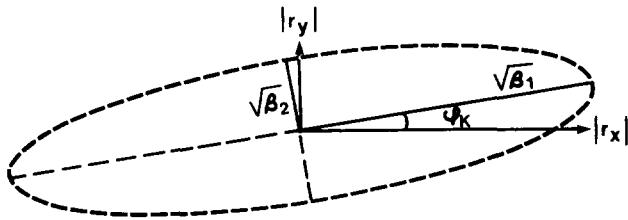


FIG. 4. Polarization of reflected light from the disk surface.

rays. Thus, a large interference enhancement of $|r_y|$ occurs. It has been shown⁷ that the approximate enhancement of the polar Kerr intensity $|r_y|^2$ over its value in a semi-infinite sample is $E \sim 8\alpha t / (1 - R)^2$ where R and α are the reflectance and absorption coefficient of semi-infinite sample, respectively, and t , the thickness of the thin absorbing layer, is typically less than 100 Å. Thus, for reasonable values of these parameters, $E \sim 10-10^2$, and the importance of device structure for obtaining maximum signal to noise during magneto-optic readout is intuitively obvious.

The mathematical framework needed to describe these effects is set up by decomposing the incident linearly polarized light into the two circularly polarized normal modes.

$$a_x = \frac{1}{2}(a_x + ia_y) + \frac{1}{2}(a_x - ia_y) = \frac{1}{2}(a^+ + a^-). \quad (2)$$

Here a_x and a_y are unit vectors along the X and Y directions. On reflection, each of the above components will be attenuated by the corresponding reflectivity. Let us use complex numbers r^+ and r^- to identify the amplitude reflectivities for left and right circularly polarized components, respectively. These of course are readily obtained, as discussed in the appendix, from n^\pm of the materials that constitute the layers of the device. The reflected field can then be written as

$$r_x a_x + r_y a_y = \frac{1}{2} r^+ (a_x + ia_y) + \frac{1}{2} r^- (a_x - ia_y). \quad (3)$$

In general, the reflected light is elliptically polarized (see Fig. 4). We define the Kerr angle φ_k as the angle between the major axis of the ellipse and the X axis. If the field component polarized along the major axis has intensity β_1 , and that along the minor axis has intensity β_2 , one can write the reflected amplitude in the following equivalent form:

$$r_x a_x + r_y a_y = [\beta_1^{1/2} (\cos \varphi_k a_x + \sin \varphi_k a_y) + \beta_2^{1/2} \exp(\pm i\pi/2) (\sin \varphi_k a_x - \cos \varphi_k a_y)] \exp(i\delta). \quad (4)$$

Here δ is a constant phase angle and can be determined, along with β_1, β_2 , and φ_k , by equating the right hand sides of Eqs. (3) and (4). The sign of $\pi/2$ in Eq. (4) determines the direction of rotation around the ellipse and must be deduced likewise.

All we need in our later analysis is β_1, β_2 , and $\varphi = |\varphi_k|$. These parameters can be expressed in terms of r^+ and r^- , independent of δ and the sign of $\pi/2$. The following results can be easily verified:

$$r_x = \frac{1}{2}(r^+ + r^-), \quad (5a)$$

$$r_y = \frac{1}{2}i(r^+ - r^-), \quad (5b)$$

$$\beta_1 = \frac{1}{2}(|r_x|^2 + |r_y|^2 + |r_x^+|^2 + |r_y^+|^2), \quad (5c)$$

$$\beta_2 = \frac{1}{2}(|r_x|^2 + |r_y|^2 - |r_x^+|^2 - |r_y^+|^2), \quad (5d)$$

$$\cos(2\varphi) = (|r_x|^2 - |r_y|^2) / |r_x^+|^2 + |r_y^+|^2. \quad (5e)$$

In the following sections we will refer to β_1, β_2 , and φ as disk parameters, keeping in mind the fact that they can always be determined from the more basic optical parameters of the constituent layers.

III. SPECTRAL ANALYSIS OF THE READ SIGNAL

Figure 5 shows a portion of a magneto-optical disk which is located in the XY plane; the presence of reverse magnetized domains is also indicated. A narrow beam of linearly polarized light, propagating in the Z direction and moving with velocity v along the X direction, is used for the retrieval of data. The beam is Gaussian and its intensity distribution in the XY plane can be expressed as

$$I(x,y,t) = (P_0/\pi r_0^2) \exp\{-[(x-vt)^2 + (y-y_0)^2]/r_0^2\}. \quad (6)$$

Here P_0 is the beam's total power, r_0 is the beam's radius at the e^{-1} point, and y_0 is the y coordinate of the track being read.

If the disk is uniform, its parameters β_1, β_2 , and φ will be constant over the entire XY plane. Define a function $Z(x,y)$ with only two values: "+1" when the magnetization at (x,y) points up and "-1" when the magnetization points down. One can then write

$$\varphi_k(x,y) = Z(x,y)\varphi. \quad (7)$$

With this notation the optical power collected at one of the photodetectors in Fig. 2 is

$$P_1(t) = \frac{1}{2} \int \int_{-\infty}^{\infty} I(x,y,t) \{ \beta_1 \sin^2[\theta + Z(x,y)\varphi] + \beta_2 \cos^2[\theta + Z(x,y)\varphi] \} dx dy. \quad (8a)$$

The power collected at the other detector will then be

$$P_2(t) = \frac{1}{2} \int \int_{-\infty}^{\infty} I(x,y,t) \{ \beta_1 \sin^2[\theta - Z(x,y)\varphi] + \beta_2 \cos^2[\theta - Z(x,y)\varphi] \} dx dy. \quad (8b)$$

Knowing the optical energy delivered to the detectors, one must in principle be able to determine the power spectral

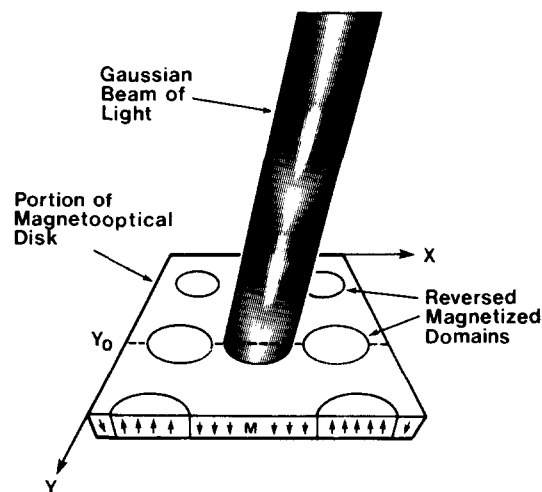


FIG. 5. Coordinate system for the spectral analysis of the read signal.

density of the output signal (in volt²/Hz), which is defined as

$$S_x(\omega) = \lim_{T \rightarrow \infty} \mathbf{E} \left[\left(\frac{1}{T} \int_{-T/2}^{T/2} x(t) \exp(-i\omega t) dt \right)^2 \right]. \quad (9)$$

The expectation in Eq. (9) is taken over the space of random functions $x(t)$. The signal $x(t)$ is the difference between the outputs of the two photodetectors and can be written as

$$x(t) = x_1(t) - x_2(t) = \sum_{k_1} (qRA)G_{k_1}h(t-t_{k_1}) - \sum_{k_2} (qRA)G_{k_2}h(t-t_{k_2}). \quad (10)$$

The subscripts 1 and 2 identify the corresponding photodetectors. In the above equation q is the electronic charge; R is the resistance in each photodetector branch; A is the amplifier's gain; G_k is the internal gain of the photodiode associated with the k 'th released electron; $h(t)$ is the impulse response of the filter, and t_k is the instant at which the k 'th electron has been released. The summations in Eq. (10) are over all electrons that contribute to the signal at time t . By substituting for $x(t)$ in Eq. (9) one arrives at

$$S_x(\omega) = \lim_{T \rightarrow \infty} \mathbf{E} \left[\left(\frac{1}{T} \int_{-T/2}^{T/2} \sum_{k_1=1}^{K_1} (qRA)G_{k_1}H(\omega)\exp(-i\omega t_{k_1}) - \sum_{k_2=1}^{K_2} (qRA)G_{k_2}H(\omega)\exp(-i\omega t_{k_2}) dt \right)^2 \right]. \quad (11)$$

Here $H(\omega) = \int_{-\infty}^{\infty} h(t)\exp(-i\omega t) dt$, and K_1 and K_2 are the total number of electrons released in the interval $[-T/2, +T/2]$ in photodetectors 1 and 2, respectively. T is assumed to be very large compared to the width of $h(t)$. Equation (11) can be expanded as

$$S_x(\omega) = (qRA)^2 |H(\omega)|^2 \lim_{T \rightarrow \infty} \mathbf{E} \left[\left(\frac{1}{T} \left(\sum_{k_1=1}^{K_1} G_{k_1}^2 + \sum_{k_2=1}^{K_2} G_{k_2}^2 + \sum_{k_1 \neq k_1'} G_{k_1} G_{k_1'} \exp[-i\omega(t_{k_1} - t_{k_1'})] + \sum_{k_2 \neq k_2'} G_{k_2} G_{k_2'} \exp[-i\omega(t_{k_2} - t_{k_2'})] - \sum_{k_1=1}^{K_1} \sum_{k_2=1}^{K_2} G_{k_1} G_{k_2} \{ \exp[-i\omega(t_{k_1} - t_{k_2})] + \exp[-i\omega(t_{k_2} - t_{k_1})] \} \right) \right)^2 \right]. \quad (12)$$

The expectation in Eq. (12) is over K_1 , K_2 , and all t_{k_1} , G_{k_1} , t_{k_2} , and G_{k_2} 's. We determine this expectation in several steps, fixing some of the random variables in each step and taking the conditional expectation over the remaining ones. First, let us fix K_1 , K_2 , and all t_{k_1} 's and t_{k_2} 's. Since the photodetector gain for one electron is independent of that for other electrons, the result of taking conditional expectations over G_{k_1} 's and G_{k_2} 's will be

$$S_x(\omega) = (qRA)^2 |H(\omega)|^2 \lim_{T \rightarrow \infty} \mathbf{E} \left[\left(\frac{1}{T} \left(\langle G^2 \rangle (K_1 + K_2) + \langle G \rangle^2 \sum_{k_1 \neq k_1'} \exp[-i\omega(t_{k_1} - t_{k_1'})] + \langle G \rangle^2 \sum_{k_2 \neq k_2'} \exp[-i\omega(t_{k_2} - t_{k_2'})] - \langle G \rangle^2 \sum_{k_1=1}^{K_1} \sum_{k_2=1}^{K_2} \{ \exp[-i\omega(t_{k_1} - t_{k_2})] + \exp[-i\omega(t_{k_2} - t_{k_1})] \} \right) \right)^2 \right]. \quad (13)$$

Here $\langle G \rangle$ and $\langle G^2 \rangle$ are the first two moments of photodetector gain. In the absence of photomultiplication both moments are equal to 1.

In Eq. (13) we now fix K_1 and K_2 and determine the conditional expectation over the t_{k_1} 's and the t_{k_2} 's. Due to the Poisson nature of photodetection, all t_{k_1} 's and t_{k_2} 's are conditionally independent⁸ and their probability density functions are proportional to $P_1(t)$ and $P_2(t)$ [See Eq. (8)]. Calculation of these conditional expectations leads to

$$S_x(\omega) = (qRA)^2 |H(\omega)|^2 \lim_{T \rightarrow \infty} \mathbf{E} \left[\left(\frac{1}{T} \left\{ \langle G^2 \rangle (K_1 + K_2) + \langle G \rangle^2 K_1 (K_1 - 1) \int \int P_1(t) P_1(t') \times \exp[-i\omega(t - t')] dt dt' / \left[\int P_1(t) dt \right]^2 + \langle G \rangle^2 K_2 (K_2 - 1) \int \int P_2(t) P_2(t') \times \exp[-i\omega(t - t')] dt dt' / \left[\int P_2(t) dt \right]^2 - \langle G \rangle^2 K_1 K_2 \int \int [P_1(t) P_2(t') + P_1(t') P_2(t)] \times \exp[-i\omega(t - t')] dt dt' / \left[\int P_1(t) dt \int P_2(t) dt \right] \right\} \right)^2 \right], \quad (14)$$

where the limits of integrations are from $-T/2$ to $+T/2$. Finally, the expectation will be taken over K_1 and K_2 which are Poisson random variables with parameters $\lambda_1 = (\eta/h\nu) \int P_1(t) dt$ and $\lambda_2 = (\eta/h\nu) \int P_2(t) dt$, respectively. [η is the quantum efficiency of photodetectors and $h\nu$ is the photon energy.] For a Poisson random variable K with parameter λ it can be shown that $\mathbf{E}[K] = \lambda$ and $\mathbf{E}[K(K-1)] = \lambda^2$; therefore

$$S_x(\omega) = (qRA)^2 |H(\omega)|^2 \times \lim_{T \rightarrow \infty} \mathbf{E} \left[(\eta/h\nu) \langle G^2 \rangle \left\{ \frac{1}{T} \int [P_1(t) + P_2(t)] dt \right\} + (\eta/h\nu)^2 \langle G \rangle^2 \times \left\{ \frac{1}{T} \int \int [P_1(t) - P_2(t)] [P_1(t') - P_2(t')] \times \exp[-i\omega(t - t')] dt dt' \right\} \right]. \quad (15)$$

$P_1(t)$ and $P_2(t)$ can now be replaced in the above equation to

yield

$$S_x(\omega) = (qRA)^2 |H(\omega)|^2 \left\{ \frac{1}{2}(\eta/h\nu)(\beta_1 - \beta_2) \langle G^2 \rangle \right. \\ \times \{ [(\beta_1 + \beta_2)/(\beta_1 - \beta_2)] - \cos(2\Theta)\cos(2\varphi) \} \\ \times \lim_{T \rightarrow \infty} \left[(1/T) \int_{-T/2}^{T/2} dt \int_{-\infty}^{\infty} \int_{-\infty}^{\infty} I(x,y,t) dx dy \right] \\ + \frac{1}{2}(\eta/h\nu)^2 (\beta_1 - \beta_2)^2 \langle G \rangle^2 \sin^2(2\Theta) \sin^2(2\varphi) \\ \times \lim_{T \rightarrow \infty} \mathbf{E} \left[(1/T) \left| \int_{-T/2}^{T/2} \exp(-i\omega t) \right. \right. \\ \left. \left. \times \int_{-\infty}^{\infty} \int_{-\infty}^{\infty} Z(x,y) I(x,y,t) dx dy dt \right|^2 \right] \right\}. \quad (16)$$

Substituting for $I(x,y,t)$ from Eq. (6) and defining the function $Z^*(x,y)$ as

$$Z^*(x,y_0) = (\pi r_0^2)^{-1/2} \int_{-\infty}^{\infty} Z(x,y) \exp[-(y-y_0)^2/r_0^2] dy, \quad (17)$$

one arrives at the following equation for the power spectral density:

$$S_x(\omega) = (qRA)^2 |H(\omega)|^2 \{ (\eta P_0/2h\nu)(\beta_1 - \beta_2) \langle G^2 \rangle \\ \times \{ [(\beta_1 + \beta_2)/(\beta_1 - \beta_2)] - \cos(2\Theta)\cos(2\varphi) \} \\ + (\eta P_0/2h\nu)^2 (\beta_1 - \beta_2)^2 \langle G \rangle^2 \sin^2(2\Theta) \sin^2(2\varphi) \\ \times \exp[-\frac{1}{2}(\omega r_0/v)^2] S_Z(\omega) \} \quad (18)$$

in which $S_Z(\omega)$ is the power spectral density of the desired signal

$$S_Z(\omega) = \lim_{T \rightarrow \infty} \mathbf{E} \left[(1/T) \left| \int_{-T/2}^{T/2} Z^*(vt,y_0) \exp(-i\omega t) dt \right|^2 \right]. \quad (19)$$

Note that the spread of the Gaussian beam in the Y direction affects the ideal signal, $Z(x,y)$, through Eq. (17). In the limit when r_0 approaches zero we will have $Z^*(x,y_0) = Z(x,y_0)$ and neither smoothing nor cross talk between tracks occurs. The spread of the beam in the X direction, however, affects the signal through the factor $\exp[-\frac{1}{2}(\omega r_0/v)^2]$ in Eq. (18). This is a bell-shaped function that attenuates the high frequency components of the signal more than the low frequency ones. Roughly speaking frequencies above $\omega = v/r_0$ will be strongly affected. Thus a smaller r_0 will reduce this effect while a larger v does not change it. This is due to the fact that the bandwidth of the signal itself increases linearly with v [see Eq. (19)].

In addition to the spectrum of the useful signal, the power spectral density in Eq. (18) contains a constant shot noise level. This is similar to the white noise spectral density usually generated by thermal fluctuations in the electronic circuitry. In fact, because of the independence of thermal fluctuations from the signal and because of their additive nature, one can add their spectral density (a constant level N_0) to the shot noise density, and lump them together in the expression for the power spectral density of total noise

$$S_N(\omega) = |H(\omega)|^2 [N_0 + (qRA)^2 (\eta P_0/2h\nu) \\ \times (\beta_1 - \beta_2) \langle G^2 \rangle \\ \times \{ [(\beta_1 + \beta_2)/(\beta_1 - \beta_2)] - \cos(2\Theta)\cos(2\varphi) \}]. \quad (20)$$

The filter $H(\omega)$ can be designed to minimize the effects of smoothing and/or optimize the signal to noise ratio. Its primary task, however, must be to eliminate the components of noise which fall outside the signal bandwidth.

IV. SIGNAL TO NOISE RATIO

In the previous section we derived expressions for the spectral densities of signal and noise. By integrating over all frequencies, one obtains the following expressions for the total signal power S and the total noise power N :

$$S = [(\eta P_0/2h\nu)(qRA)(\beta_1 - \beta_2) \langle G \rangle \sin(2\Theta) \sin(2\varphi)]^2 \\ \times \int_{-\infty}^{\infty} \exp[-\frac{1}{2}(\omega r_0/v)^2] |H(\omega)|^2 S_Z(\omega) d\omega, \quad (21)$$

$$N = \left\{ N_0 + (qRA)^2 (\eta P_0/2h\nu)(\beta_1 - \beta_2) \langle G^2 \rangle \right. \\ \times \left. \left[[(\beta_1 + \beta_2)/(\beta_1 - \beta_2)] - \cos(2\Theta)\cos(2\varphi) \right] \right\} \\ \times \int_{-\infty}^{\infty} |H(\omega)|^2 d\omega. \quad (22)$$

We now define the following parameters:

$$2B = \int_{-\infty}^{\infty} |H(\omega)|^2 d\omega, \quad (23)$$

$$n_{eq} = N_0/(qRA)^2, \quad (24)$$

$$F_G = \langle G^2 \rangle / \langle G \rangle^2, \quad (25)$$

where B can be interpreted as the system's bandwidth, n_{eq} as the equivalent rate of generation of thermal electrons prior to amplification, and F_G as the excess noise factor of the diodes. For avalanche detectors F_G obeys the following relation⁹:

$$F_G = k \langle G \rangle + (1-k)(2 - \langle G \rangle)^{-1}, \quad (26)$$

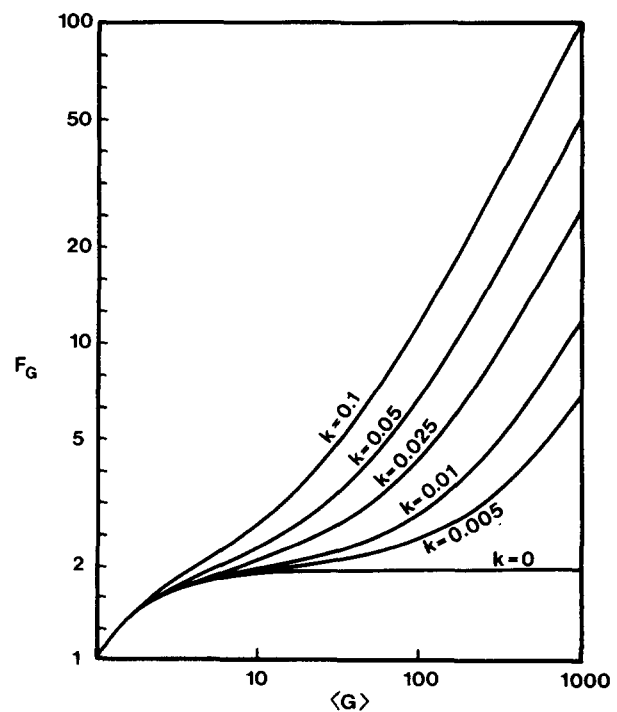


FIG. 6. Noise factor vs average gain for avalanche photodiodes.

where κ is a constant parameter known as the ionization ratio of the diode. Figure 6 shows the dependence of F_G on $\langle G \rangle$ for different values of k . Note in particular the increasing nature of F_G with the average gain.

The signal to noise ratio can now be expressed as

$$\text{SNR} = \frac{\frac{1}{2}(\eta P_0/h\nu)(\beta_1 - \beta_2)\sin^2(2\theta)\sin^2(2\varphi)}{2B(F_G\{[(\beta_1 + \beta_2)/(\beta_1 - \beta_2)] - \cos(2\theta)\cos(2\varphi)\} + 2\langle G \rangle^{-2}\{n_{\text{eq}}/[(\eta P_0/h\nu)(\beta_1 - \beta_2)]\})} \quad (27)$$

The factor $\int \exp[-\frac{1}{2}(\omega r_0/v)^2]|H(\omega)|^2 S_z(\omega) d\omega$ has been set equal to unity in the above equation for the following reason. In the ideal case, where $r_0 = 0$ and $H(\omega)$ does not distort the signal, the value of the integral is equal to 1. In a practical case, however, although this value might slightly differ from unity, it would be constant and would not vary with the parameters we seek to optimize. Therefore, as long as we are interested in the relative values of SNR, it makes

sense to set this constant equal to 1.

The signal to noise ratio can now be maximized with respect to θ . Equation (27) can be written for this purpose as

$$\text{SNR}(\theta) = \frac{1}{2}\gamma\sin^2(2\theta)/[1 - \alpha\cos(2\theta)], \quad (28)$$

where

$$\gamma = \frac{(\eta P_0/h\nu)(\beta_1 - \beta_2)\sin^2(2\varphi)}{2B(F_G[(\beta_1 + \beta_2)/(\beta_1 - \beta_2)] + 2\langle G \rangle^{-2}\{n_{\text{eq}}/[(\eta P_0/h\nu)(\beta_1 - \beta_2)]\})}, \quad (29)$$

$$\alpha = \frac{F_G\cos(2\varphi)}{F_G[(\beta_1 + \beta_2)/(\beta_1 - \beta_2)] + 2\langle G \rangle^{-2}\{n_{\text{eq}}/[(\eta P_0/h\nu)(\beta_1 - \beta_2)]\}}, \quad (30)$$

and clearly $\gamma \geq 0$ and $|\alpha| \leq 1$. It is easy to show that the optimum value of θ is given by

$$\cos(2\theta) = \alpha/[1 + (1 - \alpha^2)^{1/2}], \quad (31)$$

and that the maximum value of SNR, obtained by replacing Eq. (31) in Eq. (28), can be expressed as

$$\text{SNR} = \gamma/[1 + (1 - \alpha^2)^{1/2}]. \quad (32)$$

A modified version of the basic differential detection

scheme which is used in practice replaces the beam splitter and the two analyzers of the system of Fig. 2 with a single polarizing beam splitter (See Fig. 7). The advantage of this new version is that the reflected light need not be split before reaching the analyzers and this results in a more efficient use of the read power P_0 . The disadvantage is that θ is now fixed at 45° and cannot be optimally adjusted. The signal to noise ratio for the modified system is obtained from Eq. (27) by setting $\theta = 45^\circ$ and replacing P_0 with $2P_0$, i.e.,

$$\text{SNR}^\circ = \frac{(\eta P_0/h\nu)(\beta_1 - \beta_2)\sin^2(2\varphi)}{2B(F_G[(\beta_1 + \beta_2)/(\beta_1 - \beta_2)] + \langle G \rangle^{-2}\{n_{\text{eq}}/[(\eta P_0/h\nu)(\beta_1 - \beta_2)]\})}. \quad (33)$$

SNR° in the above equation is clearly greater than γ in Eq. (29) which is in turn greater than SNR in Eq. (32). The modified version is therefore superior to the basic system in terms of signal to noise ratio and our attention will thus be restricted to that in the remainder of this paper.

Finally, by replacing for β_1 , β_2 , and φ from Eqs. (5) in Eq. (33) we obtain

$$\text{SNR}^\circ = \frac{4(\eta P_0/h\nu)|r_x|^2|r_y|^2\cos^2(\Phi_{rx} - \Phi_{ry})}{2B\{F_G(|r_x|^2 + |r_y|^2) + \langle G \rangle^{-2}[n_{\text{eq}}/(\eta P_0/h\nu)]\}}, \quad (34)$$

where Φ_{rx} and Φ_{ry} are the phase angles of the complex numbers r_x and r_y . For a maximum signal to noise ratio Eq. (34) immediately suggests several system requirements. First, the read power P_0 should be as large as possible. Obviously, how-

ever, P_0 cannot be made very large because the heat induced in the disk will then reduce the signal sharply and may even erase the recorded spots. For a given disk structure, therefore, P_0 has an upper limit. Second, the phase difference between r_x and r_y should be eliminated. This can be done by the introduction of a phase plate with appropriate relative phase delay between the x and y directions of polarization in the path of the reflected light. An arrangement such as that shown in Fig. 7 leaves the magnitude of r_x and r_y unperturbed but eliminates the phase difference between them. For the combination of disk and the phase plate, therefore, $\beta_2 = 0$ or equivalently $\cos^2[\Phi_{rx} - \Phi_{ry}] = 1$. The presence of this phase plate will be assumed in the remainder of this article. Third, the avalanche gain $\langle G \rangle$ should be optimized. The denominator of Eq.(34) is a function of $\langle G \rangle$ and can be minimized with respect to it. The optimum gain can be shown to be

$$\langle G \rangle_{\text{opt}} = \begin{cases} 1 & \text{if } n_{\text{eq}} \leq \frac{1}{2}(\eta P_0/h\nu)(|r_x|^2 + |r_y|^2), \\ [(a^2 + b^3)^{1/2} + a]^{1/3} - [(a^2 + b^3)^{1/2} - a]^{1/3} & \text{if } n_{\text{eq}} \geq \frac{1}{2}(\eta P_0/h\nu)(|r_x|^2 + |r_y|^2), \end{cases} \quad (35)$$

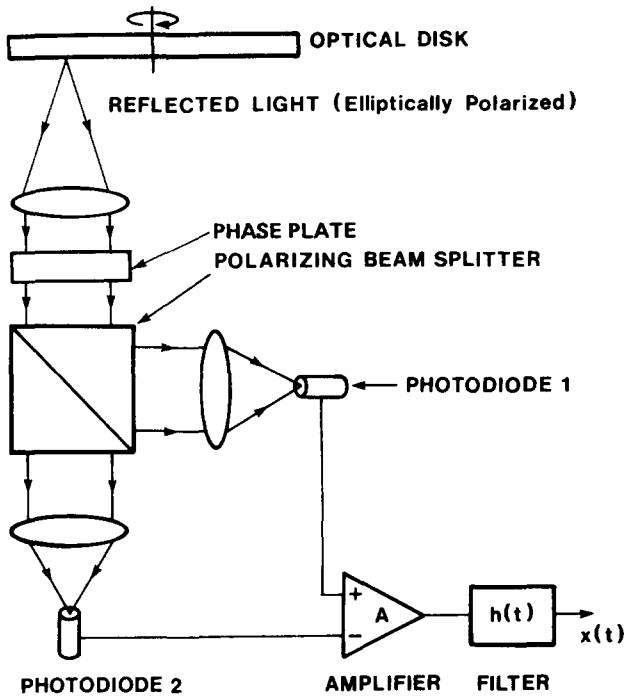


FIG. 7. Schematic diagram of the modified differential readout system.

where $a = n_{eq} / [\kappa(\eta P_0 / h\nu)(|r_x|^2 + |r_y|^2)]$ and $b = (1 - \kappa) / 3\kappa$. Finally, the structure of the disk should be optimized. With the aid of an appropriate interference device, it is possible to increase $|r_y|$ at the expense of $|r_x|$. The optimum structure then corresponds to a compromise between $|r_x|$ and $|r_y|$ that results in the maximum signal to noise ratio.

V. INTERFERENCE ENHANCEMENT OF THE KERR EFFECT

We now apply the foregoing results to examine the role of disk structure in the overall performance of the differential readout system. For concreteness, we take the system of Fig. 7 characterized by the parameters given in Table I. We also assume that each interference device is deposited on a glass substrate and has a typical magneto-optic material such as MnBi as one layer, SiO₂ or SiO for thin dielectric layers, and Al for the reflecting layer. The optical constants used are shown in Table II. The quantitative results are therefore quite specific. Nevertheless, many of the trends observed are independent of the parameters chosen, and this

allows us to make numerous general conclusions.

As a base line for discussion of our later data, we show in Fig. 8 our results for a single magnetic layer on a glass substrate. We have found the values of the avalanche gain $\langle G \rangle$ and the phase retardation required for the phase plate, represented by $(\Phi_{r_x} - \Phi_{r_y})$, that are required to maximize SNR for each magnetic film thickness. The resulting values of $|r_x|^2$ and $|r_y|^2$ are also shown.

There are numerous points to note. At thicknesses above 1600 Å, where the MnBi layer is optically thick, all the parameters are constant as expected, and SNR is about 14 db. Moreover, the phase difference between r_x and r_y is quite small, and the removal of the phase plate would not reduce SNR appreciably. At smaller thicknesses, interference effects within the metal layer become important and lead to a maximum SNR of 16.5 db, although in contrast to the thick film result, an appropriately chosen phase plate is essential. The origin of this increase, relative to the value for a thick film, may be traced directly to the enhancement of $|r_y|^2$ since from Eq. (34) $\text{SNR} \sim |r_y|^2$ for $|r_y|^2 \ll |r_x|^2$. We may therefore expect to obtain significant improvements in SNR with multilayer interference devices specifically designed to increase $|r_y|^2$, and our earlier qualitative arguments suggest that a trilayer-like device would be most effective from this point of view.

In Fig. 9 we show the quadrilayer device that has been studied. The overcoating has been added both to make it possible to fabricate the device (since oxidation of the very thin magnetic layer must be prevented) and to lend a further degree of flexibility (to be discussed later) that is absent for the trilayer. However, the intuitive ideas given earlier that suggest exceptional performance for the trilayer carry over naturally to this quadrilayer case. Figure 10 then shows the results for a device in which the intermediate and overcoat layers are SiO₂. A computer search was used to establish the values of the intermediate layer and overlayer thicknesses, t_i and t_c , respectively, that maximize SNR for each thickness of the magnetic film. The corresponding optimum values of $\langle G \rangle$ and $(\Phi_{r_x} - \Phi_{r_y})$ were calculated as before. Again at large thicknesses beyond 1600 Å, SNR, $|r_x|^2$ and $|r_y|^2$ are constant, and the increase of 4db in SNR over its corresponding value in the single film represents the effect of the (antireflecting) overlayer on the size of $|r_y|^2$. The intermediate and reflecting layers in this thick-film region are inconsequential since they are optically inaccessible. At smaller thicknesses, however, they make a significant contribution

TABLE I. Numerical values for the parameters of the differential detection system.

| Parameter | Definition | Numerical value |
|-----------|--|---------------------------|
| η | Quantum efficiency of photodiodes | 0.85 |
| P_0 | Laser read power | $2 \mu W$ |
| λ | Wavelength of light | 8400 Å |
| B | Bandwidth | 10 MHz |
| k | Ionization ratio of photodiodes | 0.02 |
| n_{eq} | Equivalent rate of generation of thermal electrons | 10^{15}sec^{-1} |

TABLE II. Optical constants of the materials.

| Material | n^+ | n^- |
|------------------|--------------|--------------|
| SiO ₂ | 1.50 | 1.50 |
| SiO | 2.00 | 2.00 |
| Al | 2.00 + 7.10i | 2.00 + 7.10i |
| MnBi | 3.77 + 3.92i | 3.56 + 3.79i |

to the performance of the structure as can be seen from the increase in $|r_y|^2$ and SNR near 800 Å where t_c is constant. Thus the improvement in the performance of the device is the result of the intermediate layer appropriately coupling the light reflected from the Al layer back into the magnetic film. At even smaller thicknesses, where the qualitative arguments for the enhancement of r_y become appropriate, SNR climbs to a maximum of 22.5 db, an increase of 8.5 db over the uncoated, thick film case, and of 4.5 db over the overcoated, thick film case. The maximum gain in $|r_y|^2$ relative to its uncoated bulk value is 9, which compares reasonably with the estimate $E \approx 8at / (1 - R)^2 \approx 16$ obtained earlier. This agreement in fact would be closer if $|r_y|^2$ were maximized rather than SNR, because in this regime $|r_x|^2$ is of order $|r_y|^2$ when $|r_y|^2$ is maximized, and the compromise between them is significant in maximizing SNR in Eq. (34).

A parenthetical remark should be made about the discontinuities in the slopes of the curves of Fig. 10 at around $t_f = 170$ Å. This seemingly curious behavior is merely a consequence of the nature of the function being optimized and bears no physical significance. In fact, a multitude of analytic functions can be found which exhibit a similar feature. As an illustrative example, consider the simple case of the poly-

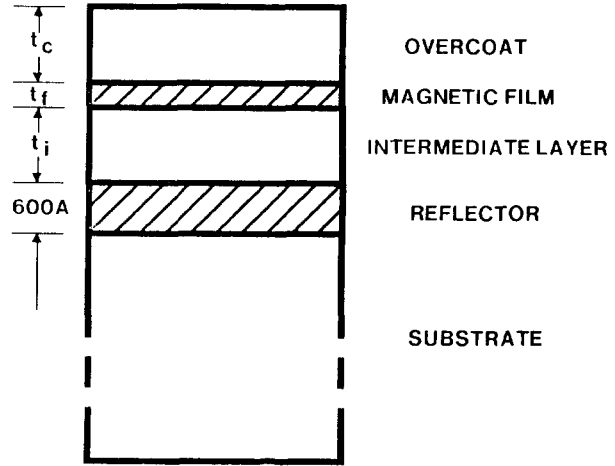


FIG. 9. Structure of the quadrilayer disk.

nominal function

$$P(X, Y) = 12X^2Y(Y - 1) + 2XY^2(2Y - 15) - Y^3(3Y + 16)$$

for $0 < X < 4$. Then as shown in Fig. 11, the value of Y that maximizes the polynomial at each X clearly shows a discontinuity in slope at $X = 1$. Below $X = 1$, there are three extrema with one an absolute maximum, while for $1 < X < 4$ there is but one maximum. The discontinuity in slope is caused by the transition from the maximum in one region to the maximum in the other. Numerically we find just this behavior in the more complicated function that was examined in determining the results in Fig. 10.

The results of optimization for a quadrilayer which has

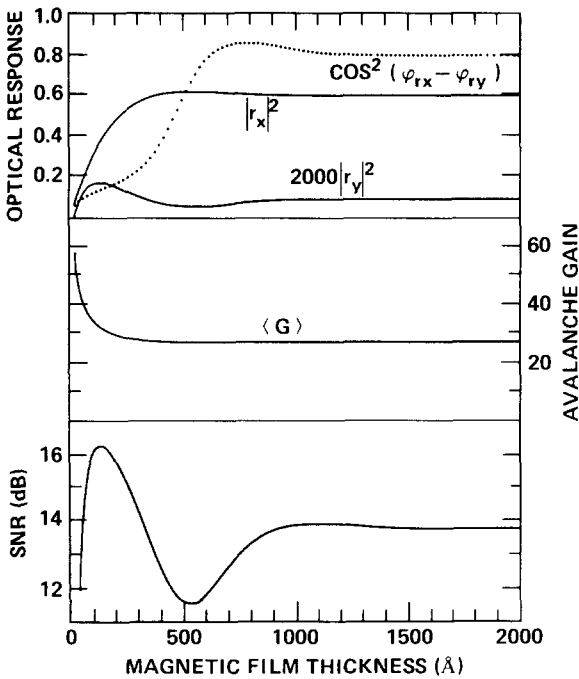


FIG. 8. Characteristics of readout: Film on glass substrate.

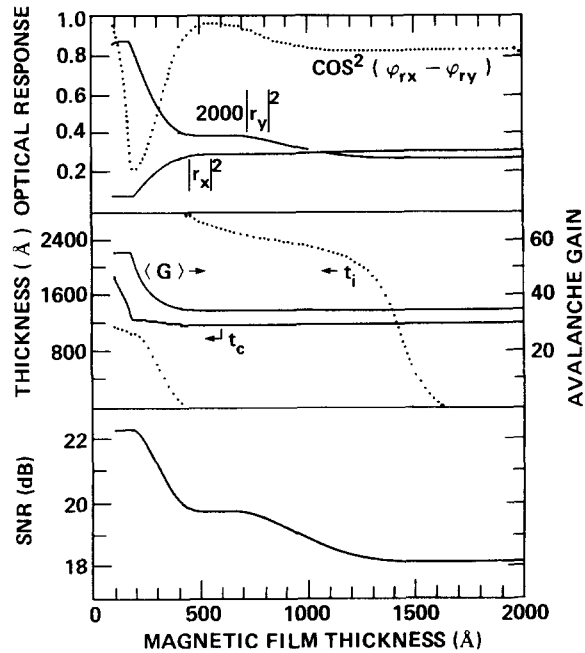


FIG. 10. Characteristics of readout: quadrilayer with SiO₂ for dielectric layers.

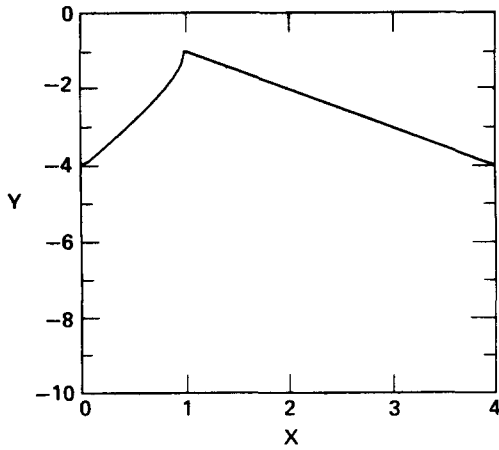


FIG. 11. Plot of the values of Y that maximize the polynomial $P(X, Y)$ at each X .

$$P(X, Y) = 12X^2Y(Y - 1) + 2XY^2(2Y - 15) - Y^3(3Y + 16).$$

SiO for intermediate and overlayers are presented in Fig. 12. Qualitatively, the results are identical to those of the previous case, but there are a few important quantitative differences. For instance, the plateau in SNR between 400 and 700 Å magnetic film thickness is now raised by about 2 db so that the difference between the absolute maximum, and this level is now only 1 db. This effect is mainly due to the change in the refractive index of the overcoat; using SiO₂ or any other dielectric as the intermediate layer has no significant effect on SNR, presumably because this layer merely creates an appropriate phase retardation. There is, therefore, much more flexibility in the design of this structure which could be of value in optimizing its performance as far as other system parameters are concerned.

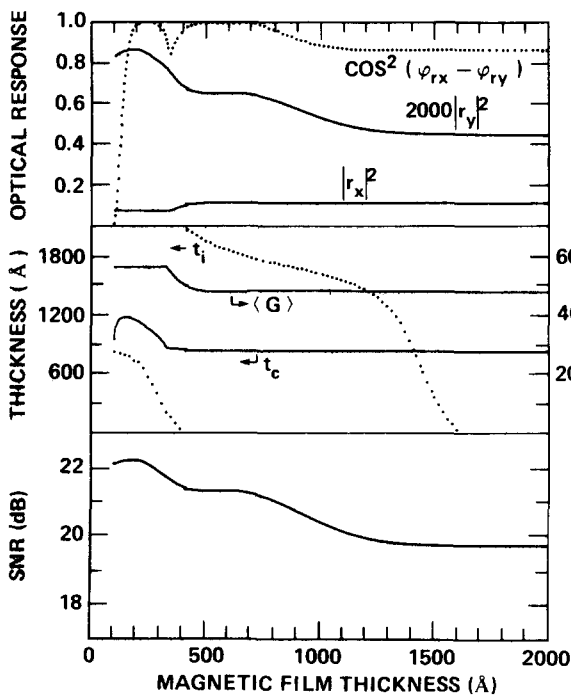


FIG. 12. Characteristics of readout: quadrilayer with SiO for dielectric layers.

VI. CONCLUDING REMARKS

In this paper we have begun a theoretical study of the readout system from a magneto-optical disk, but much is still to be done. For example, our analysis has been restricted to the most fundamental sources of noise, namely, shot noise in photodetection and thermal noise in electronic circuitry. Nevertheless, our method for the power spectral density derived in Sec. III should offer a tractable approach to considering the effects of other sources of noise that may be important in any given system. Some examples might be laser instabilities, nonuniformities of the disk structure, and nonuniformities in the pattern of recorded data.

Our optimization procedures for the disk structure might also be carried out to favor aspects of the system other than signal to noise in conditions of limited laser power. This approach was taken because at the present stage of GaAs laser development, we were concerned about the availability of power for writing, and assumed that this therefore set the limit on read power. If this situation changes to one of essentially unlimited power, either through laser or media improvements, then the figure of merit for best performance must be changed to one which considers the variation of the maximum read power with structure. Nevertheless, we expect that this can be handled within the present framework.

APPENDIX: SURFACE REFLECTIVITY OF MULTILAYERS

Consider the N layer of Fig. 13 with its surface located at $Z = 0$. Starting at the substrate with $\kappa = 1$, the layers are numbered in increasing order. For the κ 'th layer we will denote the thickness by Z_κ and the complex refractive index by $n^{(\kappa)} = n_r^{(\kappa)} + in_{im}^{(\kappa)}$. When an optical plane wave propa-

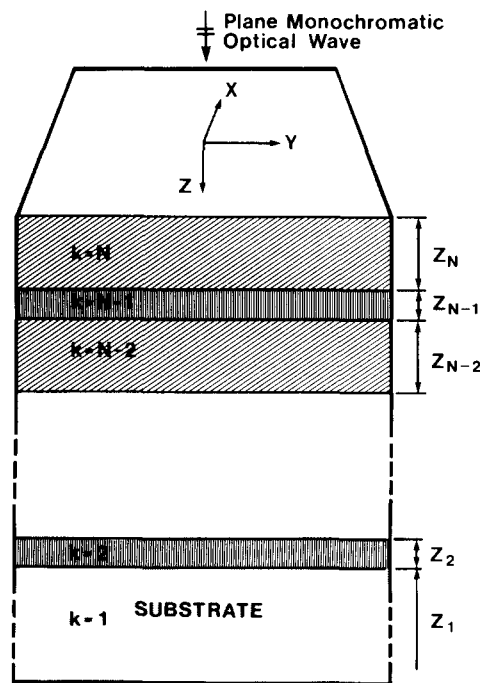


FIG. 13. Coordinate system for the calculation of reflectivity of a multilayer.

gating in the Z direction with wavelength λ_0 illuminates the surface of the multilayer, one can write the following Maxwell equations for the electric and magnetic field components in the k 'th layer¹⁰:

$$[(d^2/dZ^2) + (2\pi n^{(k)}/\lambda_0)^2]\mathbf{E}_k(Z) = 0, \quad (\text{A1a})$$

$$(d/dZ)\mathbf{E}_k(Z) - i(2\pi/\lambda_0)\mathbf{H}_k(Z) = 0. \quad (\text{A1b})$$

The general solution to these equations can be written as

$$\begin{aligned} \mathbf{E}_k(Z) = A_1^{(k)} \left\{ \exp \left[+i(2\pi n^{(k)}/\lambda_0) \left(Z - \sum_{j=k+1}^{N+1} z_j \right) \right] \right. \\ \left. + A_2^{(k)} \exp \left[-i(2\pi n^{(k)}/\lambda_0) \left(Z - \sum_{j=k+1}^{N+1} z_j \right) \right] \right\}, \end{aligned} \quad (\text{A2a})$$

$$\begin{aligned} \mathbf{H}_k(Z) = n^{(k)} A_1^{(k)} \left\{ \exp \left[+i(2\pi n^{(k)}/\lambda_0) \left(Z - \sum_{j=k+1}^{N+1} z_j \right) \right] \right. \\ \left. - A_2^{(k)} \exp \left[-i(2\pi n^{(k)}/\lambda_0) \left(Z - \sum_{j=k+1}^{N+1} z_j \right) \right] \right\}. \end{aligned} \quad (\text{A2b})$$

In the above equations $Z_{N+1} = 0$. The coefficients A_1 and A_2 must be determined in view of the continuity requirements at the boundaries. The continuity of H/E is assured if the A_2 's satisfy the following recursive relation:

$$\begin{aligned} A_2^{(k)} = \left(\frac{[n^{(k)} - n^{(k-1)}]/[n^{(k)} + n^{(k-1)}] + A_2^{(k-1)}}{1 + \{[n^{(k)} - n^{(k-1)}]/[n^{(k)} + n^{(k-1)}]\} A_2^{(k-1)}} \right) \\ \times \exp[+i(4\pi n^{(k)}/\lambda_0)z_k]; \quad 2 < k < N + 1. \end{aligned} \quad (\text{A3})$$

Since the reflected component of light in the substrate is zero one can start with $A_2^{(1)} = 0$ and determine all other A_2 's from Eq. (A3). Note that $A_2^{(N+1)}$ is the amplitude reflectivity of the surface; n_{N+1} is the refractive index of air, through which light travels to reach the multilayer, and $Z_{N+1} = 0$.

¹R. P. Hunt, IEEE Trans. Magn. **MAG-5**, 700 (1969).

²D. Chen, G. N. Otto, and F. M. Schmit, IEEE Trans. Magn. **MAG-9**, 66 (1973).

³D. Treves, J. Appl. Phys. **38**, 1192 (1967).

⁴M. Mansuripur, J. W. Goodman, E. G. Rawson, and R. E. Norton IEEE Trans. Commun. **COM-28**, 402 (1980).

⁵P. S. Pershan, J. Appl. Phys. **38**, 1482 (1967).

⁶D. O. Smith, Opt. Acta **12**, 13 (1965).

⁷G. A. N. Connell, Appl. Phys. Lett. **40**, 212 (1982).

⁸E. Cinlar, *Introduction to Stochastic Processes* (Prentice Hall, Englewood Cliffs, New Jersey, 1975).

⁹S. D. Personick, Bell Syst. Tech. J. **50**, 3075 (1971).

¹⁰J. D. Jackson, *Classical Electrodynamics* (Wiley, New York, 1967).